Chapter 7

Elliptical galaxies.

CO S 25.1

Elliptical galaxies are spheroidal stellar systems with smooth luminosity profiles. They contain old, typically metal rich stars. Unlike spiral galaxies, ellipticals exist with a very large range of stellar masses. The nature of their ISM is also different, typically consisting of tenuous hot gas detected in X-rays. The dynamics of this gas and of their observed stars both suggest that the mass of eliptical galaxies is also dominated by dark matter.

7.1 Luminosity profile (CO p. 892 & 950)

Elliptical galaxies have smooth surface brightness (SB) profiles, which in projection are ellipsoidal in shape, see examples of such profiles in Fig.7.1[1]. Average intensities as function of radius for the same galaxies are shown in Fig. 7.2. The drawn line, which fits the data well, is the **de Vaucouleurs** or '$r^{1/4}$' profile introduced previously in Eq. (3.2) for the MW's bulge[2].

$$I(r) = I_e \exp(-7.67 \left\{ (r/r_e)^{1/4} - 1 \right\}) . \tag{7.1}$$

Here, $I(r)$ is the intensity[3] at projected distance r from the centre. When

[1]Notice that in these observations, isophotes near the centre are well defined, whereas they become fainter and hence noisier in the galaxies' outskirts.

[2]The curious factor 7.67 is simply a normalisation to make r_e the half-light radius - meaning half the light is emitted interior to r_e.

[3]The amount of light emitted per unit area.

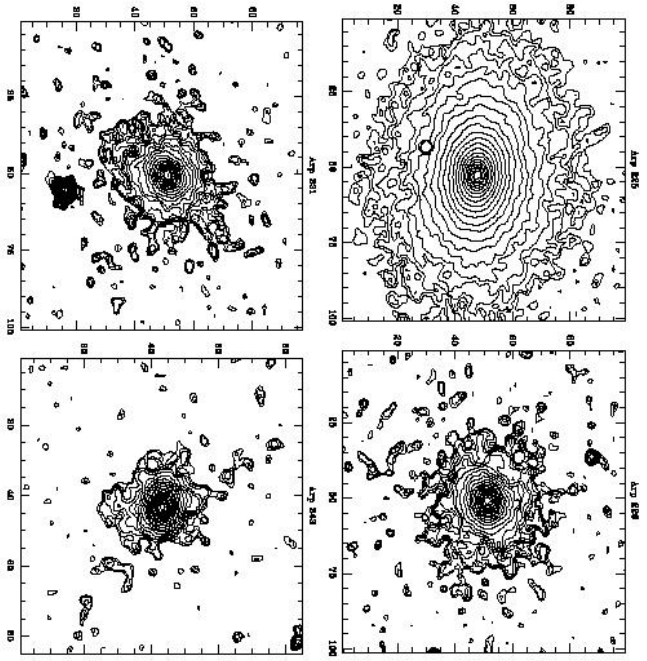

Figure 7.1: (Taken from astro-ph/0206097) Lines of constant surface brightness (isophotes) in the K-band for four elliptical galaxies. In successive isophotes, the surface brightness increases by 0.25 magnitudes.

surface brightness, $\mu = -2.5\log(I) + \text{const}$, is plotted as function of $r^{1/4}$ this profile is a straight line as in Figure 7.3. The intensity profiles of most elliptical galaxies can be fit with just the two parameters I_e and r_e.

The galaxy at the very centre of a cluster of galaxies (see next chapter) often has a very extended halo of light - much more extended than the de Vaucouleurs profile. This 'stellar halo' is build-up by the large number of mergers of the central galaxy with other elliptical galaxies. An example of such a galaxy is NGC 1399, the central in the nearby 'Fornax' cluster of galaxies, shown in Fig. 7.4. The extent of NGC 1399s halo is enormous; it can be traced[4] out to ≈ 1 Mpc.

Ellipticals also have many globular clusters (CO p. 962). Figure 7.5 is an image of NGC 1399, where an $r^{1/4}$ fit to the SB-profile of the galaxy has been subtracted. Clearly visible are 1000s of high surface brightness objects, indistinguishable on this plate from foreground stars, which are in fact globular clusters in the halo of NGC 1399.

What is the origin of the $r^{1/4}$ profile? Numerical simulations of of collisions between two spiral galaxies produce objects with surface brightness profiles resembling the $r^{1/4}$ profile. Since elliptical galaxies are found in dense environments where such collisions are frequent, it seems plausible that elliptical galaxies form from collisions between spirals galaxies. However the stellar populations of ellipticals and spirals differ: ellipticals contain mostly old and metal rich stars (see below), whereas spirals contain younger and more metal poor stars. So ellipticals may still have formed from collisions, but not collisions between *todays* spiral galaxies.

7.2 Stellar populations and ISM of ellipticals

The redder colours of elliptical galaxies is mostly due to the absence of massive and hence hot main sequence stars - itself a consequence of the fact that elliptical galaxies typically have undergone no, or very little, recent star formation. There is also a secondary effect due to the metallicity of the

[4]Which means that, given the distance to this galaxy, its extent on the night sky is comparable to that of the moon.

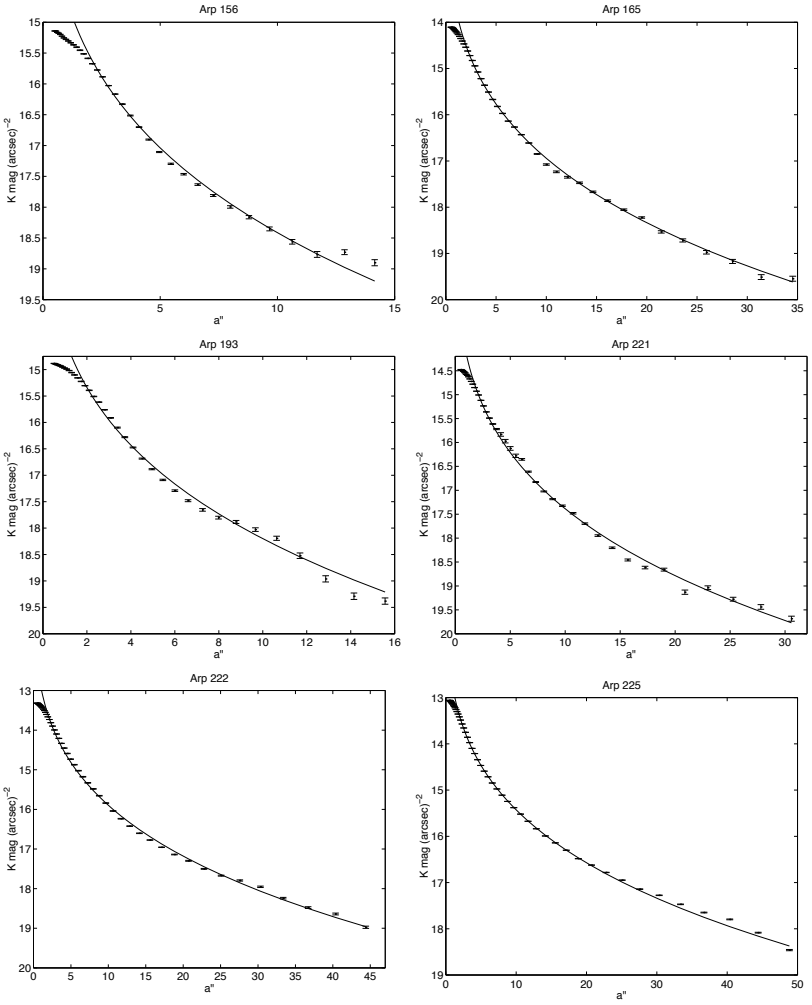

Figure 7.2: (Taken from astro-ph/0206097) Surface brightness as function of distance to the centre for the galaxies from Fig. 7.1. The drawn line is the best $r^{1/4}$ fit.

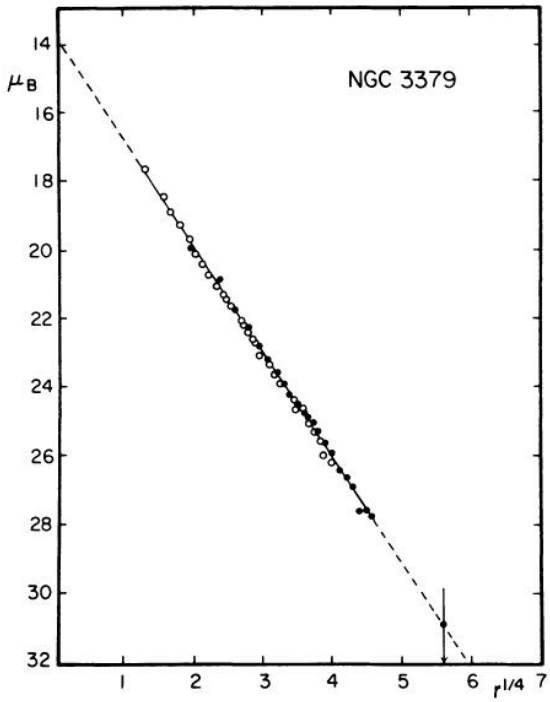

FIG. 2.—Mean E-W luminosity profile of NGC 3379 derived from McDonald photoelectric data. ●, Pe 4 data with 90 cm reflector; ○, Pe 1 data (M + P) with 2 m reflector. Note close agreement with $r^{1/4}$ law.

Figure 7.3: Luminosity profile for galaxy NGC 3379 (open symbols) compared to an $r^{1/4}$ profile (drawn line). Taken from de Vaucoleurs & Capaccioli, ApJS 40, 1979.

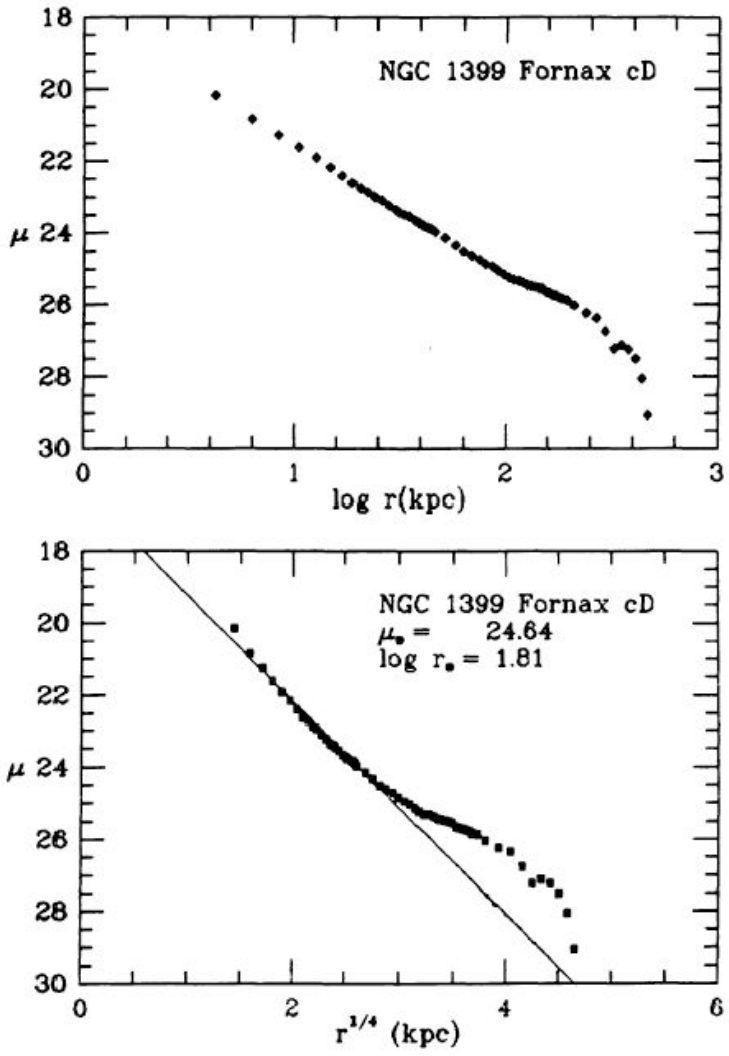

Figure 7.4: SB profile for NGC 1399 from Schombert (filled symbols; ApJS, 1989). The outer parts of the profile do not follow the $r^{1/4}$ fit (bottom panel), but are nearly a straight line in a SB-log(r) (i.e. a log $-$ log) plot (top panel), meaning the profile is close to a power-law.

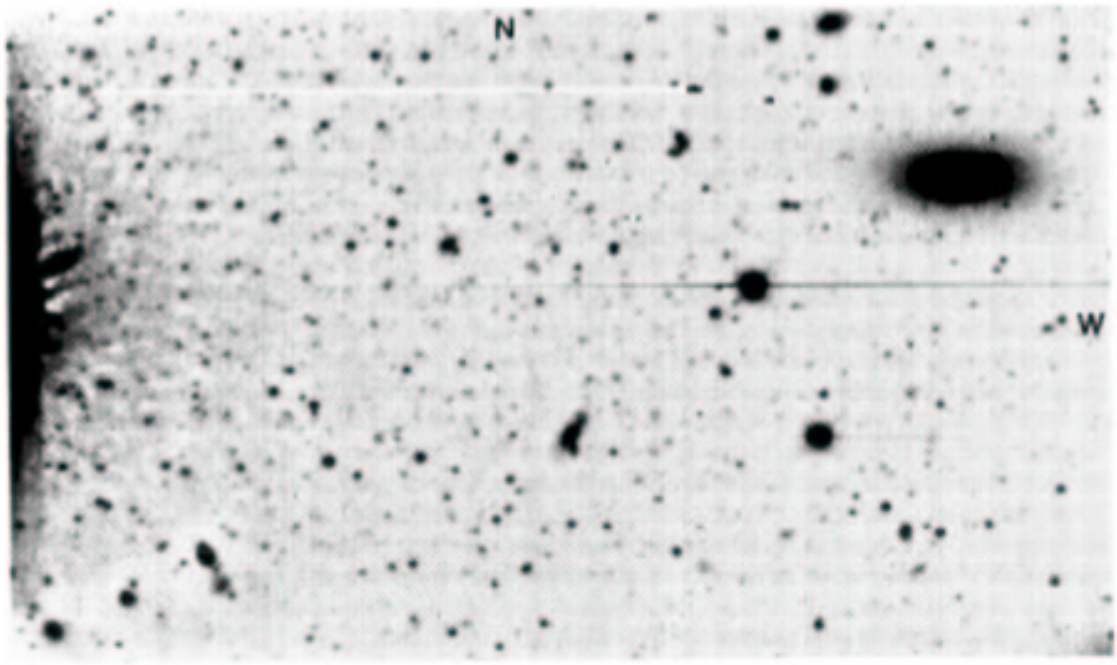

Figure 7.5: Image of NGC 1399 in the Fornax cluster of galaxies, with smooth, best fit $r^{1/4}$-profile subtracted (Bridges et al., AJ 101, 469, 1991). The centre of NGC 1399 is on the left, the object toward the top right is another galaxy in the same cluster. The other extended objects in the image are other galaxies. Clearly seen are hundreds of high SB unresolved objects - these are globular clusters associated with NGC 1399.

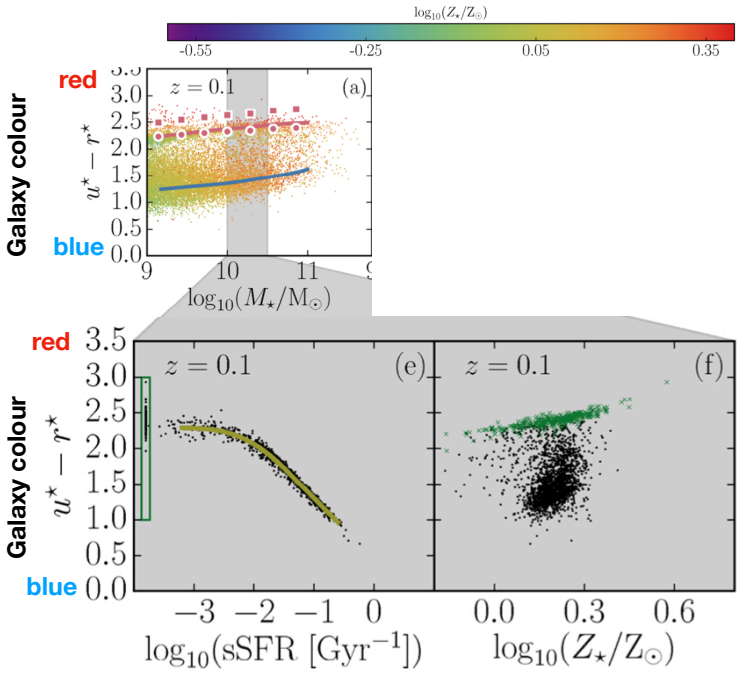

Figure 7.6: The effects of star formation and metallicity on the colours of galaxies, from Trayford+'16. The top panel shows the intrinsic $u^\star - g^\star$ colour of a galaxy plotted against its stellar mass, $M_\star$ (every dot is a galaxy), with high values of $u^\star - g^\star$ denoting a red galaxy, and low values a blue galaxy. The colour of each dot is a measure of the metallicity of the galaxy. The plot shows two sequences: a red sequence with $u^\star - g^\star \approx 2.5$ of elliptical galaxies, and a blue sequence with $u^\star - g^\star \approx 1.5$ and large scatter of star forming galaxies. The bottom left panel shows that, the higher the specific star formation rate, sSFR$\equiv \dot{M}_\star/M_\star$, the bluer the galaxy. The bottom right panel shows that for galaxies on the red sequence, redder galaxies have higher stellar metallicities, $Z_\star$.

stars: a higher metallicity makes a star redder[5]. Both effects are illustrated in Fig. 7.6.

Dust and gas The dust and cold gas that is present in the ISM of spiral galaxies is mostly absent in ellipticals. However, sometimes an elliptical galaxy may accrete a smaller galaxy and tidally tear it apart. This may result in a dust lane running across the elliptical, with the dust originating from the ISM of the ingested galaxy (see for example Fig. 7.7). Such merger events may be quite common: a number of ellipticals have faint rings of stars around them (see for example Fig. 7.8), probably also a result of such 'galactic cannibalism'.

7.3 X-rays

X-rays are absorbed by the Earth's atmosphere hence require observations from rockets or satellites. X-rays would simply be absorbed by a normal mirror and to focus them an X-ray telescope consists of many nearly parallel plates that gently nudge the incoming X-ray onto a detector [6].

Two unrelated sources contribute to the X-rays detected from ellipticals: (1) hot, tenuous gas in their interstellar medium and (2) mass-transfer in close binary stars. The physical process that produces them is the same in both cases: **thermal bremsstrahlung**. Thermal bremsstrahlung[7] is the process whereby high energy radiation (X-rays) is produced in a plasma of ions and electrons, due to the electromagnetic deflection of high-speed (thermal) hot electrons passing close to a positively charged ion. The deflection of the electron means it is accelerated, and an accelerating charge emits electromagnetic dipole radiation: this is the radiation that we observe[8] . The plasma is highly ionised because it is so hot, and the electrons are not bound to any particular ion. For this reason, thermal bremsstrahlung is sometimes

[5]Partly due to absorption of blue light in the stellar atmosphere, partly because of subtle changes in the stellar structure.

[6]See additional images on the web-page or http://chandra.harvard.edu/xray_astro/.

[7]German for 'braking radiation'.

[8]Note that the detected radiation is **not** blackbody radiation from the hot gas: the spectrum of thermal bremsstrahlung is not the same as that of a black body. Also other ions undergo electromagnetic deflections, but since they are much more massive than the electrons, their contribution to the emission is negligible.

Figure 7.7: Image of the 'CenA' galaxy, with its striking dust lane.

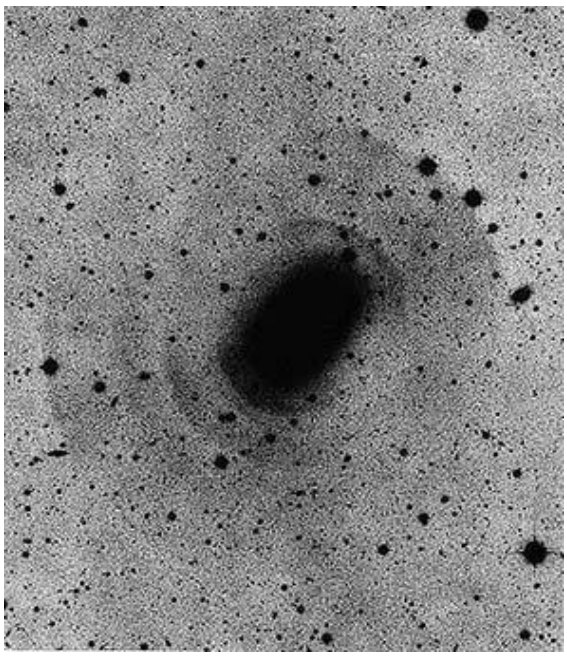

Figure 7.8: Image of NGC 3923 taken by David Malin. Several faint shells of stars appear as ripples in the outer parts of the galaxy, probably resulting from the merger of the central galaxy with a much smaller system. (see http://www.ast.cam.ac.uk/AAO/images/general/ngc3923.html)

called 'free-free' radiation.

Subtracting the X-ray point sources from the X-ray image of an elliptical galaxy - produced by its binary stars - reveals extended X-ray emission. The X-ray *emissivity* ϵ - the amount of energy radiated per unit volume - depends on density and temperature as

$$\epsilon \propto n_e \, n_i \, T^{1/2} \, , \tag{7.2}$$

where n_e and n_i are the electron and ion number densities respectively, and T is the temperature of the plasma.

Thermal bremsstrahlung produces a power-law spectrum of radiation up to a cut-off frequency $\nu_{\rm max}$ which depends on the temperature of the gas, approximately as $h\nu_{\rm max} \sim kT$. This can be use to measure the temperature of the hot plasma. In addition, observed X-ray spectra of elliptical galaxies also show *spectral lines*, where electronic transitions in some highly ionised elements present in the hot plasma contribute to the spectrum. These lines also allow a measurement of T, as well as a determination of the composition of the plasma (i.e its metal content).

7.4 Evidence for dark matter from X-rays (CO p. 1063)

The hot gas only remains bound to the elliptical galaxy because of the depth of its dark matter halo potential. If we make the reasonable assumption that the gas is in hydrostatic equilibrium with the dark matter potential, then we can measure the required halo mass - in much the same way as you did in the course on stars, as follows.

The hydrostatic equilibrium equation balances the outward force on a gas shell due to the pressure gradient across it to the inward pull due to gravity:

$$\frac{GM}{r^2} = -\frac{1}{\rho}\frac{dp}{dr} \, , \tag{7.3}$$

where M is the mass enclosed in sphere with radius r, p is pressure and ρ is density. We will assume that the gas follows an ideal equation of state, so

that

$$p = \frac{kT}{\mu m_p}\rho\,, \tag{7.4}$$

where k is Boltzman's constant, m_p the proton mass, and we take the mean molecular weight $\mu = 1/2$ - appropriate for a fully ionised hydrogen gas[9].

Observationally, the temperature T is nearly constant across the gas - so, to simplify the calculations, we will assume T to be independent of r. The rhs of Eq. (7.3) then becomes

$$\frac{1}{\rho}\frac{dp}{dr} = \frac{kT}{\mu m_p}\frac{d\ln(\rho)}{dr}\,. \tag{7.5}$$

Now multiply the lhs of Eq. (7.3) with r^2, and take the derivative,

$$\frac{d}{dr}GM = 4\pi G r^2 \rho_{\rm dm}\,, \tag{7.6}$$

where we assumed that the mass M is dominated by dark matter, with density $\rho_{\rm dm}(r)$. Combining the last two equations yields

$$4\pi G r^2 \rho_{\rm dm}(r) = -\frac{kT}{\mu m_p}\frac{d}{dr}r^2\frac{d\ln(\rho)}{dr}\,. \tag{7.7}$$

Now, numerical simulation show that the dm profile of halos is very well fitted by the following functional form[10],

$$\rho_{\rm dm}(r) = \frac{\rho_c}{r/r_s\,(1+r/r_s)^2}\,, \tag{7.8}$$

characterised by two parameters, a density, ρ_c, and a scale-radius, r_s. To find the corresponding gas density profile, consider the following *Ansatz*

$$\rho(x) = \rho_0\,\exp\left(-B\left[1-\frac{\ln(1+x)}{x}\right]\right)\,, \tag{7.9}$$

where ρ_0 and B are constants to be determined, and $x \equiv r/r_s$. A little algebra shows that

$$\frac{d}{dx}x^2\frac{d\ln(\rho(x))}{dx} = -\frac{Bx}{(1+x)^2}, \tag{7.10}$$

[9]As an exercise, compute how this would change if Helium were present as well.

[10]The famouw Navarro-Frenk & White profile, no so long ago projected on Durham cathedral during a *Lumiere* festival.

so that the rhs of Eq. (7.7) becomes

$$\frac{kT}{\mu m_p}\frac{d}{dr}r^2\frac{d\ln(\rho)}{dr} = B\frac{kT}{\mu m_p}\frac{1}{r_s^2}\frac{r/r_s}{(1+r/r_s)^2}\,. \tag{7.11}$$

Therefore

$$\rho_{\rm dm} = \frac{B}{4\pi G}\frac{kT}{\mu m_p}\frac{1}{r/r_s(1+r/r_s)^2}\,. \tag{7.12}$$

Comparison with the NWF profile of Eq.(7.9) shows that the gas distribution is in hydrostatic equilibrium with the dark matter, provided

$$\rho_c = \frac{B}{4\pi G}\frac{kT}{\mu m_p}\,. \tag{7.13}$$

Therefore measuring T and fitting B to the observed profile yields ρ_c as well as r_s - the parameters of the NFW profile. To do better, we would also have to include the contribution of both stars and gas to the potential.

7.5 Summary

After having studied this lecture, you should be able to

- describe the surface brightness profiles of Es in terms of the de Vaucouleurs profile.
- explain why we think that this profile results from galaxy encounters
- recall that Es have typically hundreds of GCs.
- explain why dust lanes in ellipticals and shells of stars around them are thought to be evidence for galactic cannibalism.
- contrast the stellar population and ISM of ellipticals with those of spirals
- describe how X-rays are detected, and explain the process with which X-rays are produced in the hot gas in ellipticals
- explain how X-ray observations can be used to infer the gravitational potential and derive the equation for hydrostatic equilibrium, relating gas profile to the underlying gravitational potential.